Shining Light on Dark Matter,
One Photon at a Time

by

Brandon Leigh Allen

Submitted to the Department of Physics
in partial fulfillment of the requirements for the degree of

Doctorate of Science in Physics

at the

MASSACHUSETTS INSTITUTE OF TECHNOLOGY

June 2019

Author . . . .
Department of Physics
May 18, 2019

Certified by. . . . .
Christoph E.M. Paus
Professor
Thesis Supervisor

Accepted by . . . .
Nergis Mavalvala
Associate Department Head for Education

Shining Light on Dark Matter,

One Photon at a Time

by

Brandon Leigh Allen

Submitted to the Department of Physics
on May 18, 2019, in partial fulfillment of the
requirements for the degree of
Doctorate of Science in Physics

Abstract

A search is conducted for new physics in final states containing a photon and missing transverse momentum in proton-proton collisions at $\sqrt{s} = 13$ TeV. The data collected by the CMS experiment at the CERN LHC correspond to an integrated luminosity of 35.9 inverse femtobarns. No deviations from the predictions of the standard model are observed. The results are interpreted in the context of dark matter production and limits on new physics parameters are calculated at 95% confidence level. For the two simplified dark matter production models considered, the observed (expected) lower limits on the mediator masses are both $950\,(1150)$ GeV for 1 GeV dark matter mass.

Thesis Supervisor: Christoph E.M. Paus
Title: Professor

Acknowledgments

This is the acknowledgements section. You should replace this with your own acknowledgements.

Contents

Chapter 1

Motivation

1.1 The Standard Model

The Standard Model (SM) of particle physics describes the physical properties and dynamics of fermions, the fundamental constituents of matter, and their interactions in the language of a Lorentz-invariant quantum field theory (QFT). The Standard Model consists of a set of fermion fields, shown in Table 1.1 and the local gauge symmetry group that acts on them

$$G_{\mathrm{SM}} = \mathrm{SU}(3)_C \times \mathrm{SU}(2)_L \times \mathrm{U}(1)_Y, \qquad (1.1)$$

which is composed of the subgroups

$$G_{\mathrm{QCD}} = \mathrm{SU}(3)_C \qquad \text{and}$$
$$G_{\mathrm{EWK}} = \mathrm{SU}(2)_L \times \mathrm{U}(1)_Y, \qquad (1.2)$$

corresponding to the strong and electroweak interactions, respectively. Each fermion field exists in a unique representation of G_{SM}, also summarized in Table 1.1. The possible represenations of $\mathrm{SU}(3)_C$ are triplet, conjugate, and singlet, denoted by $\mathbf{3}$, $\bar{\mathbf{3}}$, and $\mathbf{1}$, respectively, while the possible representations of $\mathrm{SU}(2)_L$ are doublet and singlet, denoted by $\mathbf{2}$ and $\mathbf{1}$, respectively. All fermions exist in the singlet represen-

tation of $U(1)_Y$, only distinguished by differing values of the weak hypercharge Y. Conversely, all fermions in non-singlet representations of $SU(3)_C$ and $SU(2)_L$ have the same interaction strength, a feature known as universality.

Table 1.1: The categories of SM fermions and the action of the SM local gauge symmetry group G_{SM}. Each category contains three members, one for each generation of the Standard Model. A corresponding table exists for the charge conjugated fields representing the anti-fermions. The subscripts L and R denote whether the field is left- or right-handed.

Name	Symbol	Y	$SU(2)_L$ rep.	$SU(3)_C$ rep.
Left-handed quark	q_L	$1/6$	**2**	**3**
Right-handed up-type quark	u_R	$2/3$	**1**	**3**
Right-handed down-type quark	d_R	$-1/3$	**1**	**3**
Left-handed lepton	ℓ_L	$-1/2$	**2**	**1**
Right-handed charged lepton	e_R	-1	**1**	**1**
Right-handed neutrino	ν_R	$1/6$	**1**	**1**

For each category of fermion listed in Table 1.1, there exist three generations or copies in the Standard Model, identical except for differing masses. The lepton electroweak doublets contain the left-handed charged leptons and neutrinos

$$\ell_L = \begin{pmatrix} \nu_e \\ e_L^- \end{pmatrix}, \begin{pmatrix} \nu_\mu \\ \mu_L^- \end{pmatrix}, \begin{pmatrix} \nu_\tau \\ \tau_L^- \end{pmatrix}, \tag{1.3}$$

and the right-handed lepton singlets contain the right-handed projections of the same leptons and neutrinos. The quark electroweak doublets contain the left-handed up-type and down-type quarks

$$q_L = \begin{pmatrix} u_L \\ d_L \end{pmatrix}, \begin{pmatrix} c_L \\ s_L \end{pmatrix}, \begin{pmatrix} t_L \\ b_L \end{pmatrix}, \tag{1.4}$$

and the right-handed quark singlets contain the right-handed projections of the same quarks. Quarks also exist in a strong triplet, which will be denoted with a superscript c as necessary.

1.1.1 Strong Interactions

The strong interactions of quarks and gluons are described by quantum chromodynamics (QCD), with the Lagrangian

$$\mathcal{L}_{\mathrm{QCD}} = i\bar{q}^a_f \slashed{D}^{ab} q^b_f + m_f \bar{q}^a_f q^a_f - \frac{1}{4} G^a_{\mu\nu} G^{a,\mu\nu} + \theta \frac{g_s^2}{72\pi^2} \epsilon_{\mu\nu\rho\sigma} G^{c,\mu\nu} G^{c,\rho\sigma}, \qquad (1.5)$$

where repeated indices are contracted. The q^a_f are the quark-field Dirac spinors of flavor $f \in \{u, d, c, s, t, b\}$, color $a \in \{r, g, b\}$ (the basis element of the triplet representation), and mass m_f. The first term in Equation 1.5 contains the QCD covariant derivative

$$D^{ab}_\mu = \delta^{ab} \partial_\mu - ig_s \sum_c t^{ab}_c G_{c,\mu}, \qquad (1.6)$$

where g_s is the strong interaction coupling strength, t_c are the eight 3×3 Hermitian traceless matrices that serve as the generators of the triplet representation of $\mathrm{SU}(3)_C$, and G_c are the corresponding eight gluon fields. The third term in Equation 1.5 contains the gluon field strength tensors

$$G^a_{\mu\nu} = \partial_\mu G^a_\nu - \partial_\nu G^a_\mu - g_s f^{abc} G^b_\mu G^C_\nu, \qquad (1.7)$$

where f^{abc} are the structure constants of $\mathrm{SU}(3)_C$. The non-Abelian structure of the $\mathrm{SU}(3)_C$ group allows for 3-gluon and 4-gluon interactions in addition to the quark-antiquark-gluon interactions.

The last term in Equation 1.5 violates CP conservation and produces a non-zero electric dipole moment (EDM) for the neutron. Experimental limits onthe neutron EDM constraint the QCD vaccum angle θ to be smaller than 10^{-10}. The Peccei-Quinn theory provides a possible method to force θ to zero by introducing the hypothetical axion particle. The axion is a potential dark matter candidate and will be discussed further in Section **??**.

1.1.2 Hadrons

Free quarks and gluons are not observed in nature, only in bound states called hadrons. This is a consequence of two factors: color confinement and aysmptotic freedom.

Color confinement is the hypothesis that colored objects are always confined to color singlet states and that no objects with non-zero color charge can propagate as free particles. Thus, quarks can only exist in bound states of a quark-antiquark pair or three quarks, called mesons and baryons, respectively. Since gluons carry a color charge, they are confined to hadrons as well. Confinement is a low-energy non-pertubative phenomenon, occuring only below the QCD confinement scale Λ_{QCD}. An analytic proof of color confinement does not exist currently; however, the running of the strong coupling constant $\alpha_s = g_s^2/4\pi$ provides a mechanism for it.

Due to higher-order corrections to propagators in a QFT, physical quantities such as coupling constants and masses acquire a scale-dependence, where the value of the quantity changes as a function of the probed energy scale q^2. The process of recovering scale-invariance is called renormalization and ensures that any divergent terms from the higher-order corrections cancel out in the physical values. Given the value of an arbitrary coupling constant α at some known scale μ^2, the value of α at arbitrary scale q^2 is

$$\alpha(q^2) = \frac{\alpha(\mu^2)}{1 - \alpha(\mu^2)\left[\Pi(q^2) - \Pi(\mu^2)\right]}, \tag{1.8}$$

where $\Pi(q^2)$ and $\Pi(\mu^2)$ are the self-energy correction of the propagator at scales q^2 and μ^2. While these individual terms are separately divergent, their difference is finite and calculable.

For values of q^2 and μ^2 larger than the confinement scale Λ_{QCD}, the difference between the gluon self-energy corrections to one-loop order is given by

$$\Pi_s(q^2) - \Pi_s(\mu^2) \approx -\frac{\beta}{4\pi}\ln\left(\frac{q^2}{\mu^2}\right) \tag{1.9}$$

where β depends on the number of quark and gluon loops. For N_c colors and N_f

quark flavors with mass below $|q|$,

$$\beta = \frac{11N_c - 2N_f}{12\pi}.$$ (1.10)

In the Standard Model, $N_c = 3$ and $N_f \le 6$ regardless of energy, thus β is always positive. Combining Equations 1.8 and 1.9, the evolution of α_s is given by

$$\alpha_s(q^2) = \frac{\alpha_s(\mu^2)}{1 + \beta\alpha_s(\mu^2)\ln\left(\dfrac{q^2}{\mu^2}\right)} \approx \frac{1}{\beta\ln\left(\dfrac{q^2}{\Lambda_{\mathrm{QCD}}^2}\right)}$$ (1.11)

for a sufficiently large energy scale $q^2 \gg \Lambda_{\mathrm{QCD}}^2$. Through electron-positron collisions, the value of α_s at the Z-pole has been measured to be $\alpha_s(m_Z^2) = 0.1181 \pm 0.0011$ with a corresponding confinement scale of $\Lambda_{\mathrm{QCD}} = 218\,\mathrm{MeV}$.

From Equation 1.11, we see that α_s decreases with increasing q^2. At $|q| \sim 1\,\mathrm{GeV}$, the value of α_s is of $\mathcal{O}(1)$ confining quarks and gluons to hadrons in a strongly-bound non-perturbative state. However, $|q| \gtrsim 100\,\mathrm{GeV}$, we have $\alpha_s \approx 0.1$ which is small eneough that perturbation theory can be used and quarks can be treated as quasi-free particles. This property of QCD is known as asymptotic freedom.

1.1.3 Electroweak Interactions

The electroweak interactions of fermions are described by $\mathrm{SU}(2)_L \times \mathrm{U}(1)_Y$ gauge group, with the Lagrangian

$$\mathcal{L}_{\mathrm{EWK}} = i\bar{\psi}_i \slashed{D}\psi_i - \frac{1}{4}\vec{W}_{\mu\nu}\cdot\vec{W}^{\mu\nu} - \frac{1}{4}B_{\mu\nu}B^{\mu\nu}$$ (1.12)

where repeated indices are contracted and $\psi \supseteq \{q_L, u_R, d_R, \ell_L, e_R, \nu_R\}$ is the set of SM fermions, and the gauge field tensors are given by

$$B_{\mu\nu} = \partial_\mu B_\nu - \partial_\nu B_\mu \qquad \text{and}$$
$$\vec{W}_{\mu\nu} = \partial_\mu \vec{W}_\nu - \partial_\nu \vec{W}_\mu + g\vec{W}^\mu \times \vec{W}^\nu,$$ (1.13)

where $\vec{W}_\mu$ and B_μ are the gauge fields for $SU(2)_L$ and $U(1)_Y$, respectively, and g is the coupling strength for $SU(2)_L$. The first term in Equation 1.12 contains the EWK covariant derivative

$$D_\mu = \partial_\mu - ig\vec{T} \cdot \vec{W}_\mu - ig'Y B_\mu, \qquad (1.14)$$

where g' is the coupling strength for $U(1)_Y$, Y is the $U(1)_Y$ hypercharge of the fermion field, and $\vec{T}$ are the generators of the doublet representation of $SU(2)_L$. The generators can be written in terms of the Pauli spin matrices $\vec{T} = \vec{\sigma}/2$ and only have non-zero action on left-handed particles. The values of the hypercharge Y shown in Table 1.1 are chosen such that the physical electric charge of each fermion is given by $Q = T_3 + Y$.

Notice that Equation 1.12 does not contain a Dirac mass term like that found in Equation 1.5. This is because the term

$$m\bar{\psi}\psi = m\left(\bar{\psi}_L\psi_R + \bar{\psi}_R\psi_L\right) \qquad (1.15)$$

mixes the left-handed and right-handed fermions leading to a Lagrangian that is no longer invariant under $SU(2)_L$. As the observed fermions are not massless, the Lagrangian given in Equation 1.12 is incomplete and an additional mechanism needs to be introduced to produce non-zero fermion masses.

1.1.4   Electroweak Symmetry Breaking

Spontaneous electroweak symmetry breaking provides the mechanism we need, as well as providing masses to the weak gauge bosons. The $SU(2)_L$ symmetry is broken by introducing a left-handed complex scalar doublet ϕ with $Y_\phi = 1/2$ to the Lagrangian in the following manner

$$\mathcal{L}_{\text{EWK}} \mapsto \mathcal{L}_{\text{EWK}} + |D_\mu\phi|^2 + \mu^2\phi^2 - \lambda|\phi|^4. \qquad (1.16)$$

We choose to write this complex doublet, known as the complex Higgs field, in terms of four real-valued fields so that

$$\phi = \frac{1}{\sqrt{2}} \begin{pmatrix} \phi_1 + i\phi_2 \\ \phi_3 + i\phi_4 \end{pmatrix}. \tag{1.17}$$

Fortunately, the two self-interaction terms create a Higgs potential with a degenerate global minimum at the vacuum expectation value (vev)

$$v \equiv \langle |\phi| \rangle = \sqrt{\frac{\mu^2}{\lambda}}, \tag{1.18}$$

and through gauge rotations we set $\langle \phi_{1,2,4} \rangle = 0$, removing three degrees of freedom and producing three massless Nambu-Goldstone bosons. The remaining degree of freedom is the real Higgs field H which expresses small peturbations around the vev in the third component of the complex Higgs field $\phi_3 = v + H$.

The kinetic term in Equation 1.16 couples the complex Higgs field to the EWK gauge bosons as follows at the vev

$$|D_\mu \phi|^2 = \frac{v^2}{8} \left[\left(gW_\mu^1 \right)^2 + \left(gW_\mu^2 \right)^2 + \left(g'B_\mu - gW_\mu^3 \right)^2 \right]. \tag{1.19}$$

Diagonalizing this term gives rise to the three massive weak bosons and the massless photon that we observe in nature:

$$\begin{array}{rl|l}
W_\mu^\pm \equiv \frac{1}{\sqrt{2}} \left(W_\mu^1 \mp W_\mu^2 \right) & m_W = \frac{1}{2}vg \\
Z_\mu \equiv \cos\theta_{\mathrm{W}} W_\mu^3 - \sin\theta_{\mathrm{W}} B_\mu & m_Z = \frac{1}{2}v\sqrt{g^2 + (g')^2} \\
A_\mu \equiv \sin\theta_{\mathrm{W}} W_\mu^3 + \cos\theta_{\mathrm{W}} B_\mu & m_A = 0,
\end{array} \tag{1.20}$$

where $\tan\theta_{\mathrm{W}} = g'/g$. With this, we rewrite Equation 1.12 in terms of the observed

electromagnetic, charged weaked, and neutral weak currents as follows:

$$\mathcal{L}_{\mathrm{EWK}} = \bar{\psi}_i \left(i\slashed{\partial} - eQ\slashed{A}\right)\psi_i - \frac{g}{2\sqrt{2}}\bar{\psi}_i\left(T^+\slashed{W}^+ + T^-\slashed{W}^-\right)\psi_i - \frac{1}{2}m_W^2 W_\mu^+ W^{-\mu}$$
$$- \frac{g}{2\cos\theta_{\mathrm{W}}}\bar{\psi}_i(g_V - g_A\gamma^5)\slashed{Z}\psi_i - \frac{1}{2}m_Z^2 Z_\mu Z^\mu, \qquad (1.21)$$

where $e = g'\cos\theta_{\mathrm{W}}$ is the charge of the electron, $T^\pm = (T_1 \mp iT_2)/\sqrt{2}$ are the weak isospin raising and lowering operators, and $g_V = T_3$ and $g_A = T_3 - 2Q\sin^2\theta_{\mathrm{W}}$ are the vector and axial-vector couplings for the neutral weak current.

We can also expand Equation 1.16 about the vev giving us the following Higgs Lagrangian

$$\mathcal{L}_H = \frac{1}{2}\partial_\mu H \partial^\mu H - \frac{1}{2}m_H^2 H^2 + \frac{m_H^2}{2v}H^3 + \frac{2m_W^2}{v}W_\mu^+ W^{-\mu}H + \frac{m_Z^2}{v}Z_\mu Z^\mu H$$
$$+ \frac{m_H^2}{8v^2}H^4 + \frac{m_W^2}{v^2}W_\mu^+ W^{-\mu}H^2 + \frac{m_Z^2}{2v^2}Z_\mu Z^\mu H^2, \qquad (1.22)$$

where $m_H = \mu\sqrt{2}$. Thus, we see that the real Higgs field H has trilinear and quartic couplings to itself and the weak gauge bosons with coupling strengths proportional to the mass squared of the appropriate boson. This suggests a way to introduce fermion masses through the Higgs field.

1.1.5   Fermion Masses

Introducing Yukawa couplings between the complex Higgs field ϕ and the SM fermion fields enables us to add mass terms for the fermions. First, we start with the terms for charged leptons,

$$\mathcal{L}_{\mathrm{Y}}^{\mathrm{leptons}} = -\bar{\ell}_L Y_e \phi e_R - \bar{e}_R Y_e \phi^\dagger \ell_L, \qquad (1.23)$$

where Y_e is the Yukawa matrix for the charged leptons. In general, Yukawa matrices and thus mass matrices are non-diagonal and hence we need to convert from the electroweak eigenstates $f_{L,R}$ to the mass eigenstates $\tilde{f}_{L,R} = U_{L,R}^f f_{L,R}$ where $U_{L,R}^f$ is a

unitary matrix. With this we rewrite Equation 1.23 in terms of the mass eigenstates

$$\mathcal{L}_{\mathrm{Y}}^{\mathrm{leptons}} = -\bar{\tilde{\ell}}_L U_L^e Y_e \phi U_R^{e\dagger} \tilde{e}_R - \bar{\tilde{e}}_R U_R^e Y_e \phi^\dagger U_L^{e\dagger} \tilde{\ell}_L$$
$$= -\bar{\tilde{\ell}}_L \tilde{Y}_e \phi \tilde{e}_R - \bar{\tilde{e}}_R \tilde{Y}_e^\dagger \phi^\dagger \tilde{\ell}_L, \tag{1.24}$$

where $\tilde{Y}_e = U_L^e Y_e U_R^{e\dagger}$ is the diagonalized Yukawa matrix for the charged leptons. After electroweak symmetry breaking, these terms become

$$\mathcal{L}_{\mathrm{Y}}^{\mathrm{leptons}} = -\frac{v+H}{\sqrt{2}} \left(\bar{\tilde{e}}_L \tilde{Y}_e \tilde{e}_R + \bar{\tilde{e}}_R \tilde{Y}_e^\dagger \tilde{e}_L \right)$$
$$= -\left(1 + \frac{H}{v} \right) \left(\bar{\tilde{e}}_L \tilde{M}_e \tilde{e}_R + \bar{\tilde{e}}_R \tilde{M}_e^\dagger \tilde{e}_L \right)$$
$$= -\tilde{M}_e \bar{e} e - \frac{\tilde{M}_e}{v} \bar{e} e H, \tag{1.25}$$

where $\tilde{M}_e = v\tilde{Y}_e/\sqrt{2}$ is the diagonalized mass matrix for the charged leptons and e is the set of massive Dirac spinors for the charged leptons.

From Equation 1.25, we see that the Yukawa couplings between the complex Higgs field ϕ and the charged leptons result in a Dirac mass term and a coupling to the real Higgs field H that is proportional to the mass of the charged leptons and the vev. The same procedure is used to introduce mass terms for the down-type quarks whereas for the neutrinos and up-type quarks we must use the conjugate doublet $\phi_c = -i\sigma_2 \phi^*$ in place of ϕ to obtain the same result.

1.1.6 Flavor Mixing

For the charged leptons and up-type quarks, it is possible to define a basis of simultaneous electroweak and mass eigenstates, so in practice $\tilde{Y}_{e,u} = Y_{e,u}$ as $U_L^{e,u} = U_R^{e,u} = \mathbf{I}$. However, it is not possible to do this for the neutrinos at the same time as the charged leptons or for the down-type quarks at the same time as the up-type quarks.

In Equation 1.21, the charged current term involves interactions between the up-type and down-type quarks and is not preserved under the transform $f \to \tilde{f}$. Writing

this in terms of the mass eigenstates we have

$$\mathcal{L}_{\text{CC}} = -\frac{g}{2\sqrt{2}} \left(\bar{u}_L T^+ W^+ d_L + \bar{d}_L T^- W^- u_L \right)$$
$$= -\frac{g}{2\sqrt{2}} \left(\bar{u}_L T^+ W^+ V_{\text{CKM}} \tilde{d}_L + \bar{\tilde{d}}_L T^- W^- V_{\text{CKM}}^\dagger u_L \right), \tag{1.26}$$

where $V_{\text{CKM}} = U_L^{u\dagger} U_L^d$ is the Cabibbo-Kaboyshi-Maskawa matrix and $u_L = \tilde{u}_L$ by construction. The CKM matrix is unitary with four free parameters, the mixing angles between quark generations $\phi_{12} = 13.1$, ϕ_{23}, and ϕ_{13} as well as a CP-violating phase δ. In terms of these parameters, the CKM matrix is

$$V_{\text{CKM}} = \begin{pmatrix} c_{12} & s_{12} & 0 \\ -s_{12} & c_{12} & 0 \\ 0 & 0 & 1 \end{pmatrix} \times \begin{pmatrix} 1 & 0 & 0 \\ 0 & c_{23} & s_{23} \\ 0 & -s_{23} & c_{23} \end{pmatrix} \times \begin{pmatrix} c_{13} & 0 & s_{13}e^{-i\delta} \\ 0 & 1 & 0 \\ -s_{13}e^{i\delta} & 0 & c_{13} \end{pmatrix}, \tag{1.27}$$

where $s_{ij} = \sin\phi_{ij}$ and $c_{ij} = \cos\phi_{ij}$. It has been experimentally determined that the CKM is mostly diagonal with $s_{13} \ll s_{23} \ll s_{12} \ll 1$.

The equivalent mixing matrix for the neutrinos is the Pontecorvo-Maki-Nakagawa-Sakata matrix U_{PMNS}, which converts from the mass eigenstates ν_1, ν_2, and ν_3 to the electroweak eigenstates ν_e, ν_μ, ν_τ. Unlike the CKM matrix, the PMNS is non-diagonal resulting in stronger mixing in the neutrino sector. The values of the mixing angles θ_{12}, θ_{23}, and θ_{13} have been measured in neutrino oscillation experiments while the CP-violating phase δ' has not yet been directly measured. From cosmological measurements, it is known that the sum of the neutrino masses is less than one eV.

1.1.7 Summary

The Standard Model has a total of 26 free parameters and 17 physical particles. The parameters are the twelve Yukawa couplings for the fermions, the four parameters of the CKM matrix, the four parameters of the PMNS matrix, the three coupling constants g_s, g, and g', the Higgs vacuum expectation value v, the Higgs mass m_H, and the QCD vacuum angle θ.

Table 1.2: The free parameters of the Standard Model, not including masses.

Parameter	Description	Value
ϕ_{12}	CKM 12-mixing anlge	13.1°
ϕ_{23}	CKM 23-mixing angle	2.4°
ϕ_{13}	CKM 13-mixing angle	0.4°
δ	CKM CP-violating phase	0.995
$\sin^2\theta_{12}$	PMNS 12-mixing anlge	0.297
$\sin^2\theta_{23}$	PMNS 23-mixing angle	0.437
$\sin^2\theta_{13}$	PMNS 13-mixing angle	0.0214
δ'	PMNS CP-violating phase	1.35
g_s	$SU(3)_C$ coupling constant	1.221
g	$SU(2)_L$ coupling constant	0.652
g'	$U(1)_Y$ coupling constant	0.357
v	Higgs vacuum expectation value	246 GeV
θ	QCD vacuum angle	$< 10^{-10}$

Table 1.3: The physical particles of the Standard Model.

Name	Symbol	Spin	Charge	Mass
up quark	u	½	⅔	2.2 MeV
down quark	d	½	-⅓	4.7 MeV
charm quark	c	½	⅔	1.28 GeV
strange quark	s	½	-⅓	95 MeV
top quark	t	½	⅔	173 GeV
bottom quark	b	½	-⅓	4.18 GeV
electron neutrino	ν_e	½	0	-
electron	e	½	-1	511 keV
muon neutrino	ν_μ	½	0	-
muon	μ	½	-1	105 MeV
tau neutrino	ν_τ	½	0	-
tau	τ	½	-1	1.78 GeV
gluon	g	1	0	0
photon	γ	1	0	0
Z boson	Z	1	0	91.2 GeV
W boson	$W^\pm$	1	±1	80.4 GeV
Higgs boson	H	0	0	125 GeV

The physical particles are the single-particle states of the various mass eigenfields and their properties are summarized in Table 1.3. Each of the fermion fields has a corresponding anti-particle with the electromagnetic and color charges inverted. Most of these single-particle states have finite lifetimes and decay to lower energy configurations. The only particles whose decays have not been observed are the photon, the electron, the neutrinos, and the proton (a baryon of flavor content uud).

Chapter 2

The Large Hadron Collider

The Large Hadron Collider (LHC) is a circular proton-proton collider, 27 km in circumference and between 40 and 175 m below the surface, located at the European Organization for Nuclear Research (CERN) on the French-Swiss border near the city of Geneva. Designed to collide protons at a maximum center-of-mass energy $\sqrt{s} = 14\,\text{TeV}$, the LHC has delivered collisions at $\sqrt{s} = 7, 8\,\text{TeV}$ during Run 1 (2010-2012) and at $\sqrt{s} = 13\,\text{TeV}$ during Run 2 (2015-2018). While the LHC is primarily a proton-proton collider, lead (Pb) ion beams of energy of up to 2.8 TeV per nucleon are used to produce lead-lead and proton-lead collisions. In this thesis, we focus exclusively on data recorded from proton-proton collisions during Run 2.

The LHC is the final stage of the CERN accelerator complex depicted in Figure 2-1. Hydrogen atoms are stripped of their electrons and accelerated to an energy of $50\,\text{GeV}$ by the LINAC2 linear acceleration. Following this, they are injected into the Booster ring, the Proton Synchrotron (PS), and the Super Proton Synchrotron (SPS) and accelerated to 1.4, 26, and $450\,\text{GeV}$, respectively. After the SPS, the protons are injected into the two counter-circulating rings of the LHC in up to 2808 discrete bunches with a bunch spacing of $25\,\text{ns}$. The two beams intersect in eight places along the LHC with detector experiments CMS, ATLAS, LHCb, and ALICE each located at an intersection point.

The LHC is a synchrotron containing 1232 superconducting NbTi dipole magnets measuring 15 m in length, each with a peak dipole field of 8.33 Tesla. There are an

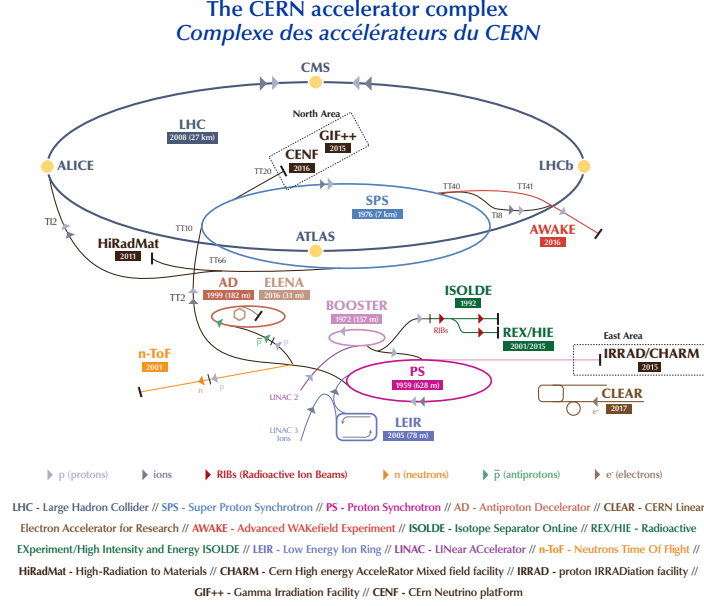**The CERN accelerator complex**
Complexe des accélérateurs du CERN

Figure 2-1: A schematic representation of the CERN accelerator complex. The LHC (dark blue) is fed protons by a chain of intermediate accelerators, beginning with LINAC2 (light pink). Reprinted from the CERN Document Server [].

additional 492 quadrupole magnets measuring 5-7 m in length which focus the beams in between the dipole magnets. Due to space limitations in the tunnels, the beam pipes are magnetically coupled and the magnets share the same superfluid liquid helium cryostatic system to achieve the 1.9K temperature required to achieve the desired magnetic field strength.

The number of events produced at the LHC is given by

$$N(pp \to X) = \int dt L(t) \sigma(pp \to X), \qquad (2.1)$$

where σ is the cross section of the process and L is the instantaneous luminosity of the machine given by

$$L = \frac{N_b^2 n_b f_{\text{rev}} \gamma}{4\pi\epsilon\beta^*} \times F, \qquad (2.2)$$

where N_b is the number of particles per bunch ($\mathcal{O}(10^1 1)$), n_b is the number of bunches per beam, f_{rev} is frequency of revolution, γ is the Lorentz factor of the beam, ϵ is transverse emittance of the beam, β^* is beta function of the beam at the collision

point, and F is the geometric luminosity reduction factor due to the crossing angle at the interaction point. The instantaneous luminosity decreases exponentially as a function of time due to N_b and n_b being reduced by collisions. The LHC is designed to deliver an initial instantaneous luminosity of $\mathcal{O}(10^{34})\,\mathrm{cm^{-2}\,s^{-1}}$.

As all known cross sections are time-independent, the total number of events is directly proportional to the integrated luminosity given by

$$L_{\mathrm{int}} = \int_0^T dt L(t) = L(0)\tau_L \left(1 - e^{-T/\tau_L}\right), \qquad (2.3)$$

where T is the time since starting collisions, $L(0)$ is the initial instantaneous luminosity, and $\tau_L \approx 15$ the characteristic beam loss timescale for the LHC. The total luminosity delivered by the LHC and recorded by CMS during the 2016 is shown in Figure 2-2.
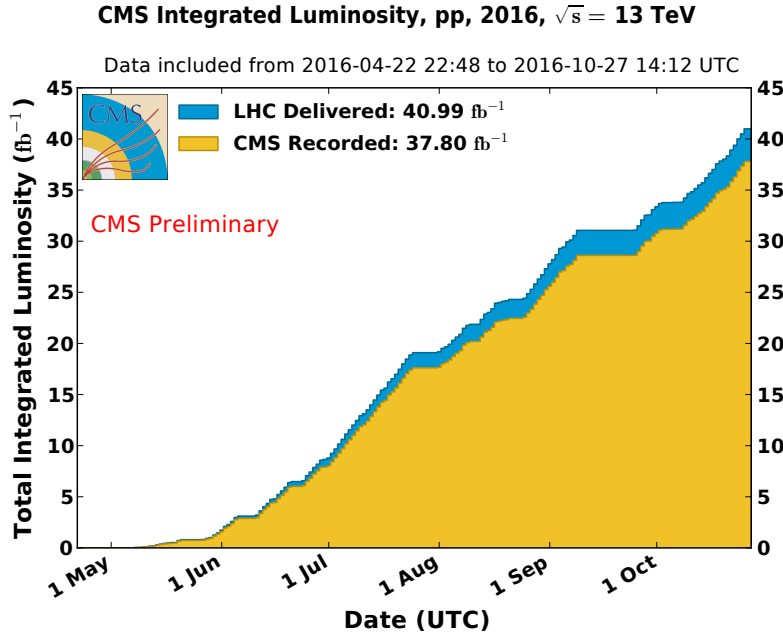

CMS Integrated Luminosity, pp, 2016, $\sqrt{s} = 13$ TeV

Data included from 2016-04-22 22:48 to 2016-10-27 14:12 UTC

LHC Delivered: 40.99 fb^{-1}
CMS Recorded: 37.80 fb^{-1}

CMS Preliminary

Figure 2-2: The total integrated luminosity of the LHC during proton-proton collisions during 2016.[] While a total luminosity of $41\,\mathrm{fb^{-1}}$ was collected, only a subset during which the detector operated optimally is used in this thesis. This corresponds to $36\,\mathrm{fb^{-1}}$ of data.

2.1 Collider Phenomenology

The proton is a composite particle consisting of valence quarks, sea quarks, and gluons, collectively referred to as partons. When colliding protons at the LHC, we are actually interested in the inelastic scattering of a pair of partons from the incident protons. Each parton a, b carries a fraction of the momentum of the incoming proton $x_{a,b}$ following the particle-dependent parton distribution functions (PDFs) $f_{a,b}$. The differential cross section for $2 \to N$ parton scattering process is given by

$$d\sigma\left(ab \to \{c_i\}\right) = \frac{(2\pi)^4}{2s} \left(\prod_i \frac{d^3 p_i}{(2\pi)^3}\right) \cdot \delta^4\left(k_a + k_b - \sum_i p_i\right) \cdot |\mathcal{M}\left(ab \to \{c_i\}\right)|^2 \quad (2.4)$$

where $k_{a,b} = x_{a,b}\sqrt{s}$ are the momenta of the incoming partons, $\{p_i\}$ are the momenta of the outgoing partons $\{c_i\}$, and $\mathcal{M}$ is the matrix element of the process.

This parton level scattering, called the hard scattering process, is perturbatively calculable through standard QFT methods. However, the hard scattering does not include any effects related to the PDFs of the incoming partons or the decay and hadronization of the outgoing partons into the final state particles (called the parton shower), both of which involve non-pertubative aspects of QCD. Fortunately, the collinear factorization theorem states that the probability of obtaining the final state $X(\Theta)$ from a hadron collision can be calculated as the product of the probability that specific partons a, b are involved in the interaction, the probability for the hard scattering to produce outgoing partons $\{c_i\}$, and the formation of final state hadrons from these outgoing partons. The factorization process is not unique and requires the choice of an arbitrary energy scale μ_F, which defines a lower bound for interactions to be considered part of the hard scattering.

Including the effects from PDFs and parton showering (PS), the general cross section for $pp \to X(\Theta)$ is

$$\frac{d\sigma}{d\Theta}\left(pp \to X(\Theta)\right) = \sum_{a,b} \int dx_a f_a(x_a, \mu_F) \cdot dx_b f_b(x_b, \mu_F)$$

$$\times d\sigma\left(ab \to \{c_i\}\right) \times D\left(\{c_i\} \to X(\Theta)\right) \quad (2.5)$$

where the sum is over the initial state partons and D is the fragmentation function that describes parton shower process resulting in the observed final state. The following sections discuss the simulation of the three main elements of Equation 2.5: the parton distribution functions f_a, the hard scattering cross section $d\sigma$, and the fragmentation function D.

2.1.1 Parton Distribution Functions

2.1.2 Hard Scattering

2.1.3 Parton Shower